ADVANCES IN ATMOSPHERIC SCIENCES, VOL. 40, MAY 2023, 843–855

• **Original Paper** •

Summer Extreme Precipitation in the Key Region of the Sichuan-Tibet Railway※

Jiali MA[1,2,3] and Xiuping YAO[*3,1]

[1]*State Key Laboratory of Severe Weather*, *Chinese Academy of Meteorological Sciences*, *Beijing* 100081, *China*

[2]*University of Chinese Academy of Sciences*, *Beijing* 100049, *China*

[3]*China Meteorological Administration Training Centre*, *Beijing* 100081, *China*

(Received 7 May 2022; revised 5 August 2022; accepted 29 August 2022)

ABSTRACT

The Sichuan-Tibet Railway, mainly located in the southeastern Qinghai-Tibet Plateau, is affected by summertime extreme precipitation (SEP). Using daily rain-gauge observations and ERA5 reanalysis data for the summers of 1979–2020, the spatiotemporal distribution characteristics of SEP in the key region of the Sichuan-Tibet Railway (28°–33°N, 90°–105°E, hereafter KR) are revealed, and the mechanism for SEP amount (SEPA) variation in the KR is investigated. The results show that SEPA in the KR contributes nearly 30% to the total summer precipitation. Regional differences are evident in SEP, justifying thresholds higher in the plateau-dominated central-western KR (CWKR) and lower in the basin-dominated eastern KR (EKR). In addition, SEP in the CWKR is less intense but more frequent than SEP in the EKR. During 1979–2020, the SEPA in the KR increased slightly while the SEPA in the CWKR increased significantly and peaked in the last decade. When anticyclonic circulation (AC) anomalies dominate the 500 hPa pattern over the Bay of Bengal and Mongolia, the southerly flow and cyclonic shear over the southeastern plateau will be strengthened, favoring more SEPA in the CWKR. When an AC anomaly dominates the 500 hPa pattern over the Bohai Sea, the low-level easterly wind over the basin will be strengthened, favoring more SEPA in the EKR. The strengthening of the ascent, water vapor convergence, and convective instability is conducive to more SEPA in the KR. Our results deepen the understanding of the characteristics and the physical mechanisms responsible for extreme precipitation in the KR.

Key words: summertime extreme precipitation, distribution characteristics, variation mechanism

Citation: Ma, J. L., and X. P. Yao, 2023: Summer extreme precipitation in the key region of the Sichuan-Tibet Railway. *Adv. Atmos. Sci.*, **40**(5), 843−855, https://doi.org/10.1007/s00376-022-2133-z.

Article Highlights:

- SEP contributes nearly 30% of the summer precipitation in the KR, and its intensity and frequency differ greatly between the CWKR and EKR.
- During the last 42 years, SEPA in the KR increased slightly, but SEPA in the CWKR increased significantly and peaked in the last decade.
- The variation of SEPA in the CWKR and EKR are influenced by significantly different circulation anomalies.

1. Introduction

The Sichuan-Tibet Railway, connecting Chengdu in the east and Lhasa in the west, is China's second "sky road" into Tibet and of critical importance in promoting the social and economic development of western China (Xue et al., 2021). With most of the railway in the Qinghai-Tibet Plateau (plateau) and the remainder in the Sichuan Basin (basin), the complexity of the geographical environment along the railway allows for geological disasters such as landslides, debris flows, and collapses to occur frequently. As a result, the Sichuan-Tibet Railway has faced great challenges during its construction, operation, and maintenance (Lu and Cai, 2019).

Extreme precipitation can potentially induce such geological disasters (Shi and Yang, 2020; Liu et al., 2021; Palin et al., 2021). Since global warming accelerated in the 1980s, there has been a significant increase in the frequency and amount of extreme precipitation (Hegerl et al., 2019; Myhre et al., 2019; Zhou et al., 2022), which resulted in a significant

※ This paper is a contribution to the special issue on the 14th International Conference on Mesoscale Convective Systems and High-Impact Weather.

* Corresponding author: Xiuping YAO
Email: yaoxp@cma.gov.cn

increase in disaster risk for China's railway infrastructure (Liu et al., 2021). Given that most of the extreme yearly precipitation occurs in summer (June–August) (Sun and Zhang, 2017; Yao et al., 2017), research on summertime extreme precipitation (SEP) along the Sichuan-Tibet Railway is of significant importance to safeguard the construction, operation, and maintenance of the railway.

Extreme precipitation along the Sichuan-Tibet Railway exhibits great spatial heterogeneity. In general, the amount of extreme precipitation in the basin is more than that in the plateau (Deng et al., 2022). During the recent half-century, the plateau has experienced a trend towards warmer and more humid conditions (Li et al., 2010) and a general increase in the frequency of extreme precipitation (Zhai and Pan, 2003). Specifically, the amount of extreme precipitation increased in the southwestern, central, northern, and eastern parts of the plateau, while it decreased in the southeastern part (Li et al., 2019; Xiong et al., 2019; Ding et al., 2021). Different from the increasing trend of extreme precipitation in most parts of the plateau, the basin has more stations with decreasing extreme precipitation than those with increasing extreme precipitation (Huang et al., 2014). The maximum 1-day precipitation significantly decreased in the western Sichuan Basin (Sun and Zhang, 2017) and the extreme precipitation frequency shows a decreasing trend in the eastern basin (Zhai and Pan, 2003). These results highlight the complex regional differences in the variation trend of extreme precipitation along the Sichuan-Tibet Railway.

Extreme precipitation is closely related to changes in the atmospheric circulation as well as the kinetics and thermodynamic factors such as ascent, water vapor convergence, atmospheric convective instability (O'Gorman and Schneider, 2009; Li et al., 2012). The mechanisms of extreme precipitation variations are mostly independent (Deng et al., 2022). Past research has demonstrated the strengthening of the Indian and East Asian summer monsoons (Zhu et al., 2015), the strengthening of the blocking high at the Ural Mountains (Feng and Wei, 2008), the weakening and northward shift of the westerly jet (Gao et al., 2014; Sun et al., 2020; Ding et al., 2021), the strengthening and northward shift of the West Pacific Subtropical High (WPSH) (Liu et al., 2016), and cyclonic circulation anomalies in the Bay of Bengal (Liu et al., 2016), all of which are conducive to the enhancement of precipitation in the plateau. The northward shift of the westerly jet in the eastern plateau is conducive to weakening the precipitation in the southern plateau (Zhao et al., 2022). The westward expansion of the WPSH, the northward shift and eastward stretching of the Iran High, the strengthening of the Indian Low, and a middle-latitude trough represent favorable circulation backgrounds for heavy precipitation in the Sichuan region (Chen et al., 2010; Hu and Li, 2015). The anticyclonic anomaly in the upper troposphere over China are conducive to the enhancement of extreme precipitation over the western Sichuan Basin (Deng et al., 2022). These results show that the circulation background for extreme precipitation varies greatly along the Sichuan-Tibet Railway.

Previous research mostly focused on either Sichuan province (or Basin) or the Qinghai-Tibet Plateau independently, and there are inconsistencies in the dataset, study period, and subregion definitions (Zhang et al., 2021). Currently, there is limited research based on the particular region along the Sichuan-Tibet Railway (hereafter, the key region of the Sichuan-Tibet Railway, referred to as KR). Therefore, the spatiotemporal distribution of SEP in the KR remains unclear, and the mechanism for SEP amount (SEPA) variation in the KR also remains unclear. Addressing these two unresolved issues is necessary to deepen the scientific understanding of the characteristics and mechanisms of SEP along the Sichuan-Tibet corridor, which helps to safeguard the Sichuan-Tibet Railway.

Therefore, by focusing on the KR, this study employs the rain-gauge precipitation data from 1979–2020 to reveal the spatiotemporal distribution characteristics of SEP in the KR, including the spatial distribution characteristics of SEP and the interannual variation characteristics of SEPA, and to investigate the cause for SEPA variation. The remainder of this paper is organized as follows: Section 2 introduces the data and methods. Section 3 reveals the spatial-temporal distribution characteristics of SEP in the KR. Section 4 investigates the mechanism for SEPA variation in the KR. Section 5 provides a summary and discussion.

2. Data and Methods

2.1. *Data*

The precipitation data used in this study is the daily precipitation data from China's national surface weather station dataset (V3.0), which consists of records collected by more than 2400 nationwide rain-gauges since 1951. The daily precipitation records the 24 h precipitation over the 24-h period from 2000 to 2000 (day+1) LST (Local Standard Time, LST = UTC + 8). It is further broken down into nighttime (2000–0800 LST) precipitation and daytime (0800–2000 LST) precipitation. This dataset is quality-controlled by the National Meteorological Information Center of China Meteorological Administration. The study period is June, July, and August of 1979–2020. To ensure the consistency and integrity of the precipitation data being used, rain-gauges built after 1979 or with a missing data ratio of more than 10% within the study period are dismissed (Zhao et al., 2018).

The atmospheric reanalysis data used in this study are the monthly averaged data from constant pressure levels from the fifth generation ECMWF (European Centre for Medium-Range Weather Forecasts) atmospheric reanalysis (ERA5 reanalysis data). The data has a spatial resolution of $0.25° \times 0.25°$, a vertical range of 1000–100 hPa, and the analysis period is June–August 1979–2020.

The topography data and the boundary data of the Qinghai-Tibet Plateau are from the Digital Elevation Model of China (1 km) (Tang, 2019) and Integration dataset of Tibet Plateau boundary (Zhang et al., 2019a), respectively. These

data can be downloaded at the National Tibetan Plateau Data Center (https://data.tpdc.ac.cn/en).

Notably, the above data have not been standardized.

2.2. *Methods*

2.2.1. *Definition of the key region of the Sichuan-Tibet Railway*

The rectangular area of 28°–33°N, 90°–105°E enclosing the Sichuan-Tibet Railway is defined as the key region of the Sichuan-Tibet Railway, which is the KR. Based on this definition, a total of 127 rain-gauges in KR are selected. Figure 1 illustrates the KR and the distribution of the rain-gauges within.

The area (28°–33°N, 90°–105°E) within the red dashed rectangular represents the KR, and the red dashed slash within the KR denotes the boundary between the central-western KR (CWKR) and eastern KR (EKR) (see the dividing details in section 3.1). The yellow dashed line denotes the Sichuan-Tibet Railway. The yellow dots represent the rain-gauges along the railway with their location names, Chengdu, Ya'an, and Kangding in Sichuan province and Qamdo, Nyingchi, Shannan, and Lhasa in Tibet, in yellow, and the green dots represent the other rain-gauges in the KR. The solid orange curve represents the boundary of the Qinghai-Tibet Plateau. The cyan curves from east to west represent Jinsha River, Lantsang River, and Yarlung Zangbo River (all within Tibet), respectively. The thin black curves represent the provincial boundaries of China. The grey shading represents the altitude according to the color bar on the right.

2.2.2. *Definition of SEP and related statistical parameters*

This study adopts the threshold method, which is widely used in defining extreme precipitation (Zhai and Pan, 2003; Zhai et al., 2005; You et al., 2008; He and Zhai, 2018), to define SEP. The details are as follows: for each rain gauge in the KR, all wet days (days with daily precipitation $\geqslant$ 0.1 mm d^{-1}) in the summers of 1979–2020 are selected and sorted by daily precipitation from smallest to largest, then the 95th percentile of the daily precipitation value is defined as the SEP threshold (R_{95}) of this rain-gauge. Precipitation larger than R_{95} is defined as SEP.

Various aspects of SEP are worth exploring, such as its frequency, intensity, total precipitation amount and its contribution to summer total precipitation, which are frequently explored in extreme precipitation research (Zhang et al., 2011). Therefore, we defined SEPD to measure the frequency of SEP, SEPA to measure SEP's total precipitation amount, SEPI to measure the mean daily precipitation (intensity) of SEP, R_{SEP} to measure the contribution of SEP to summer total precipitation (see Table 1 for details). In addition, we also formulated two parameters R_n and N_{ce} (see Table 1 for details); we use R_n to measure the nighttime portion of SEPA because nocturnal precipitation greatly contributes to the overall precipitation in the KR (Hu and Li, 2015; Pan et al., 2021), whose damage is harder to monitor and prevent compared to daytime precipitation. Yet less attention is paid to the nighttime proportion of SEP. We use N_{ce} to measure how often consecutive SEPs occur because SEPs that occur consecutively are more likely to be damaging than SEPs that occur separately (Kundzewicz et al., 2005; Webster et al., 2011; He and Zhai, 2018; Du et al., 2022).

3. Spatial-temporal distribution characteristics of SEP in the KR

3.1. *Spatial distribution characteristics of SEP in the KR*

By averaging the statistical parameters over all rain-gauges in the KR, the characteristics of the regionally averaged SEP in the KR are revealed as follows. During the past 42 years in the KR, the regionally averaged mean number of SEPD is 2.7 d yr^{-1} , accounting for 3% of summer days. The regionally averaged mean annual SEPA and mean annual summer precipitation amount is 141 mm yr^{-1} and 481 mm yr^{-1}, respectively, and thereby the regional average R_{SEP} is 29.3%, indicating that SEP contributes to nearly 30% of summer total precipitation in the KR. The regionally averaged SEPI is 54 mm d^{-1}. The regionally averaged R_n is 74%, while the regionally averaged percentage of nighttime precipitation out of the total summer precipitation is 67%, indicating that SEP has a higher nocturnal precipitation percentage than moderate summer precipitation. The regionally averaged mean annual N_{CE} is 0.2 times yr^{-1}, indicating SEP occurs in pairs once every 5 years in the KR.

SEP in the KR exhibits significant regional differences. The eastern boundary of the plateau (EBP) divides the KR into an eastern part (EKR), mostly basin terrain, and a central-western part (CWKR), mostly plateau terrain. The EKR has an R_{95} that is without exception larger than 25 mm d^{-1},

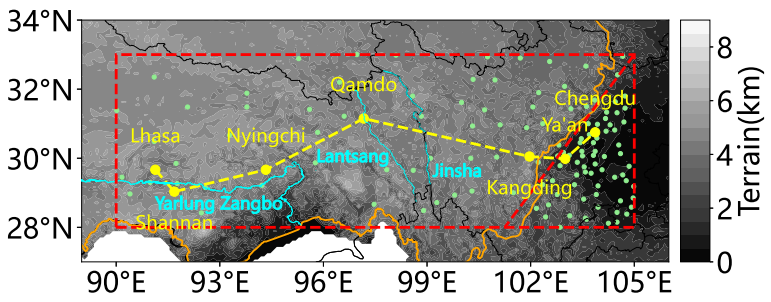

Fig. 1. Illustration of the KR and its distribution of rain-gauges.

Table 1. Related statistical parameters of SEP for each rain-gauge in the KR.

Statistical parameter (abbreviation)	Definition	Units
Summer extreme precipitation days (SEPD)	Day with daily precipitation larger than R_{95}	d for the number of SEPD
Summer extreme precipitation amount (SEPA)	The total precipitation amount SEPDs during a certain period	mm
Summer extreme precipitation intensity (SEPI)	$\text{SEPI} = \frac{\text{SEPA}}{\text{the number of SEPDs}}$ (the mean daily precipitation of SEP)	mm d^{-1}
Percentage of SEPA in summer total precipitation amount (R_{SEP})	$R_{SEP} = \frac{\text{SEPA}}{\text{summer total precipitation amount}}$, the contribution of SEP to the total summer precipitation	%
Percentage of nighttime precipitation in SEP (R_n)	$R_n = \frac{\text{total nighttime precipitation amount* of SEP}}{\text{SEPA}}$, R_n ranges from 0 to 1 with 1(0) indicating all SEP are all nighttime (daytime) precipitation	%
Number of consecutive SEP event (N_{ce})	If 2 SEPDs take place consecutively, it is defined a consecutive SEP event. N_{ce} is the count of consecutive SEP events. A zero value indicates that all SEPDs were isolated in nature and a higher N_{ce} indicates SEPDs occur more consecutively.	times

(*): The nighttime precipitation refers to 2000–0800 LST precipitation in section 2.1.

with a minimum R_{95} of 29.6 mm d^{-1}, while the CWKR has an R_{95} that is without exception smaller than 25 mm d^{-1} with a maximum R_{95} of 24.2 mm d^{-1} (Fig. 2a). These results indicate that 1) R_{95} in the EKR is much larger than that in CWKR, 2) the EBP is not only the geographic boundary but can also be regarded as the boundary of the SEP threshold in the KR. For the convenience of illustration, this boundary is denoted by the red dashed slash in Fig. 1, and 3) SEP thresholds are higher than 25 mm d^{-1} in the CWKR and lower than 25 mm d^{-1} in the EKR, which provides the scientific reference for the heavy precipitation standard of 25 mm d^{-1} for the Qinghai-Tibet Plateau (Zhang et al., 2016; Sun et al., 2021).

Further calculations show that over the past 42 years, in the EKR (CWKR), the regionally averaged mean annual summer precipitation is 604 mm yr^{-1} (343 mm yr^{-1}) (Fig. 2b); the regionally averaged mean number of SEPD is 2.5 d yr^{-1} (3.0 d yr^{-1}) (Fig. 2c); the regionally averaged mean annual SEPA is 200 mm yr^{-1} (76 mm yr^{-1}) (Fig. 2d); the regionally averaged R_{SEP} is 33% (22%) (Fig. 2e); the regionally averaged SEPI is 80 mm d^{-1} (25 mm d^{-1}) (Fig. 2f), the regionally averaged R_n is 72% (75%) (Fig. 2g); and the regionally averaged mean annual N_{CE} is 0.16 events yr^{-1} (0.23 events yr^{-1}) (Fig. 2h). To summarize, SEP in the CWKR has nearly 70% less intensity, 60% less summer precipitation amount, a smaller contribution to summer precipitation, but 20% higher frequency, a slightly higher frequency of consecutive occurrence and a slightly higher nocturnal percentage than SEP in the EKR.

3.2. *Interannual variation characteristics of SEPA in the KR*

Over the past 42 years, SEPA in the KR increased at a rate of 0.142 mm yr^{-1}, although this increase failed the significance test at the 0.1 level (Fig. 3a), thus, indicating a slight increase in SEPA in the KR during the last 42 years.

The interannual variations of SEPA in the CWKR and EKR are different. The SEPA in the EKR exhibits an increasing rate of 0.007 mm yr^{-1} (failing the significance test at 0.1 level) (Fig. 3b). In comparison, SEPA in the CWKR exhibits an increasing rate of 0.292 mm yr^{-1} (passing the significance test at 0.1 level) (Fig. 3c). Therefore, the SEPA in the EKR remained nearly the same. In contrast, SEPA in the CWKR increased significantly during the last 42 years.

To further investigate the inter-annual variation of SEPA, a heavy SEPA year and a weak SEPA year are defined using Eqs. (1–3):

$$x_{si} = \frac{x_i - \bar{x}}{s}, \tag{1}$$

$$\bar{x} = \frac{1}{n}\sum_{i=1979}^{2020} x_i, \tag{2}$$

$$s = \sqrt{\frac{1}{n}\sum_{i=1979}^{2020}(x_i - \bar{x})^2}, \tag{3}$$

where x_i is the total SEPA in year i (i = 1979, 1980, …, 2020), x_{si} is the standardized value of x_i, n is the count of years, n = 42, $\bar{x}$ is the mean annual SEPA, s is the standard deviation. Note that the x_i is the regionally averaged value, and the computing is applied on the KR, CWKR, and EKR, respectively. A year i which has $x_{si} \geqslant 1$ is defined as a heavy SEPA year, and a year i which has $x_{si} \leqslant -1$ is defined as a weak SEPA year for the region.

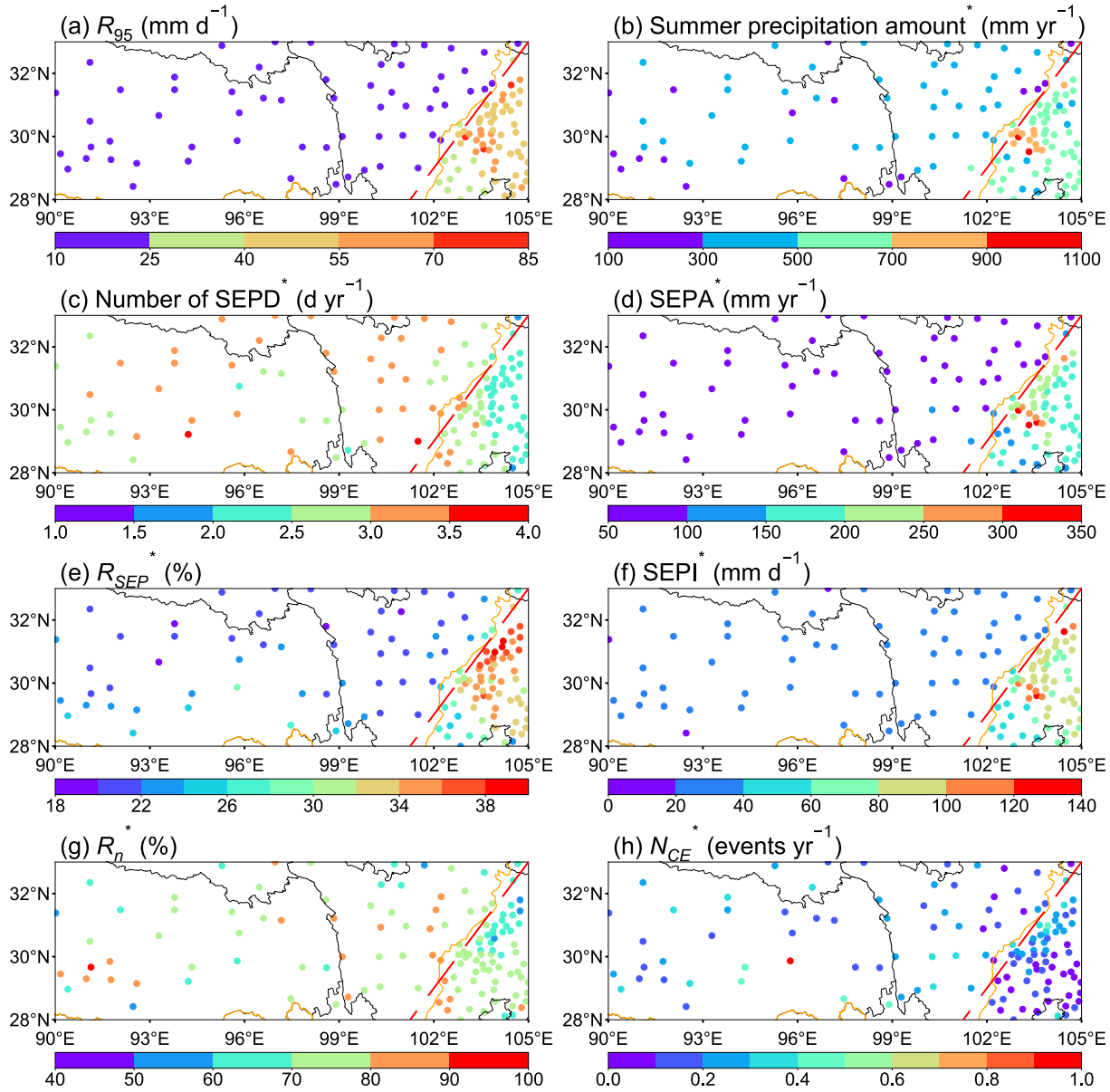

Fig. 2. Spatial distribution of (a) R_{95}, (b) summer precipitation amount, (c) number of SEPD, (d) SEPA, (e) R_{SEP}, (f) SEPI, (g) R_n and (h) N_{CE} in the KR. In each subplot, the parameter name is marked at the upper left, and * indicates that the result is the climatological mean (averaged over 1979–2020). The scattered dots represent the location of rain gauges, and their colors correspond to the magnitude with the color bar at the bottom. The red dashed diagonal line denotes the boundary between the CWKR and EKR. The other map settings are the same as Fig. 1.

On this basis, it can be seen that during the last 42 years, more than half (3) of all 5 heavy SEPA years in the KR occurred in the last decade (Fig. 3a). Specifically, more than half (4) of all 7 heavy SEPA years in the CWKR (Fig. 3c) and nearly half (3) of all 7 heavy SEPA years in the EKR occurred in the last decade (Fig. 3b). In the CWKR, the regionally averaged mean annual SEPA during 2011 to 2020 is 86 mm yr^{-1}, higher than 73 mm yr^{-1} during 1981–90, 75 mm yr^{-1} during 1991–2000 and 68 mm yr^{-1} during 2001–10 (Fig. 3c), suggesting that SEPA in the CWKR peaked in the last decade during the past 42 years. Furthermore, 2020 was the year with the most SEPA during the last 42 years for both the KR and EKR and is also the year with the most SEPA during the last decade for the CWKR.

To summarize section 3, during the last 42 years, SEP accounted for only 3% of the summer days, yet contributed to nearly 30% of summer total precipitation amount in the KR, and had a significant nocturnal tendency, constituting nearly 75% of all SEPA. On average, SEP days in the KR occurred consecutively once every five years. The KR can be subdivided by the EBP into the plateau-dominated CWKR with an R_{95} smaller than 25 mm d^{-1} and the basin-dominated EKR with an R_{95} larger than 25 mm d^{-1}. The SEP in the CWKR has a nearly 70% reduction in intensity, yet a 20% higher frequency, a slightly higher frequency of consecutive occurrence, and a slightly higher nocturnal per-

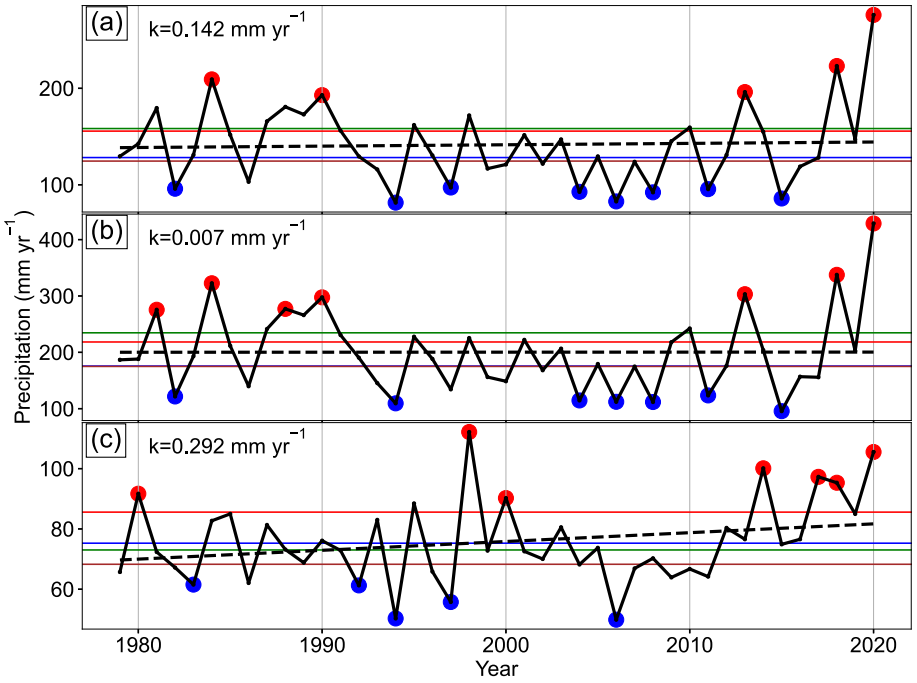

Fig. 3. Interannual variations of regionally averaged SEPA in the (a) KR, (b) EKR, and (c) CWKR from 1979 to 2020. The solid black line represents regionally averaged SEPA. The green, blue, brown, and solid red lines represent the average value from 1981 to 1990, 1991 to 2000, 2001 to 2010, and 2011 to 2020, respectively. Red and blue dots indicate the values that are bigger than +1 standard deviation and smaller than −1 standard deviation, corresponding to the heavy SEP years and the weak SEP years, respectively. The dashed black line shows the linear trend. The *K* value is the annual growth rate.

centage than the SEP in the EKR. In terms of interannual variability, the SEPA in the KR increased slightly, while the SEPA in the CWKR increased significantly during the past 42 years. More than half of all heavy SEPA years happened in the last decade, and the SEPA in the CWKR also peaked in the last decade, with 2020 having the greatest SEPA in the KR.

4. The mechanism for SEPA variation in the KR

According to section 3, the temporal variations of SEPA in the CWKR and EKR are quite different, likely indicating that the mechanisms for SEPA variation in the CWKR and EKR are also different. Therefore, they will be discussed separately. The methodology is as follows: for either the CWKR or EKR, the mean summer atmosphere anomalies of heavy SEP years and weak SEP years are composited respectively to study the impact of atmospheric circulation, ascent, water vapor convergence, and atmospheric convective instability on SEPA variation in the region.

It is worth noting that the reason for using the mean summer atmosphere to represent mean atmosphere of SEP is that the interannual variation of summer precipitation amount is highly correlated with the interannual variation of SEPA (correlation coefficient of 0.92 and passing the significance test at the 0.05 level); therefore, the mean atmospheric condition of SEP can be regarded as consistent with that of the mean summer atmosphere (Lu et al., 2021).

4.1. *The impact of atmospheric circulation*

The variation in SEPA is greatly affected by atmospheric circulation.

The circulation patterns in heavy SEP years for the CWKR are as follows. At 200 hPa, a strong anticyclonic circulation anomaly dominates the western plateau, and anomalous northerlies along with a positive divergence anomaly are found over the CWKR, which is conducive to upper-level divergence over the CWKR (Fig. 4a). At 500 hPa, the strong anticyclonic circulation anomaly over the Bay of Bengal strengthens the moist southwesterly flow into the plateau and moistens the low-level air over the CWKR. Also, the strong anticyclonic circulation anomaly in Mongolia helps to establish a geopotential anomaly pattern of "high northeast, low southwest" north of the CWKR, thereby turning the anomalous southwesterly flow in the CWKR cyclonically into anomalous southeasterly flow under the pressure gradient force and forms a low-level "cyclonic shear" flow anomaly over the CWKR (Fig. 4b).

In contrast, the circulation patterns in weak SEP years are as follows. At 200 hPa, a strong cyclonic circulation anomaly dominates the western plateau causing an anomalous southerly flow and a negative divergence anomaly over the CWKR. This pattern is detrimental to the upper-level diver-

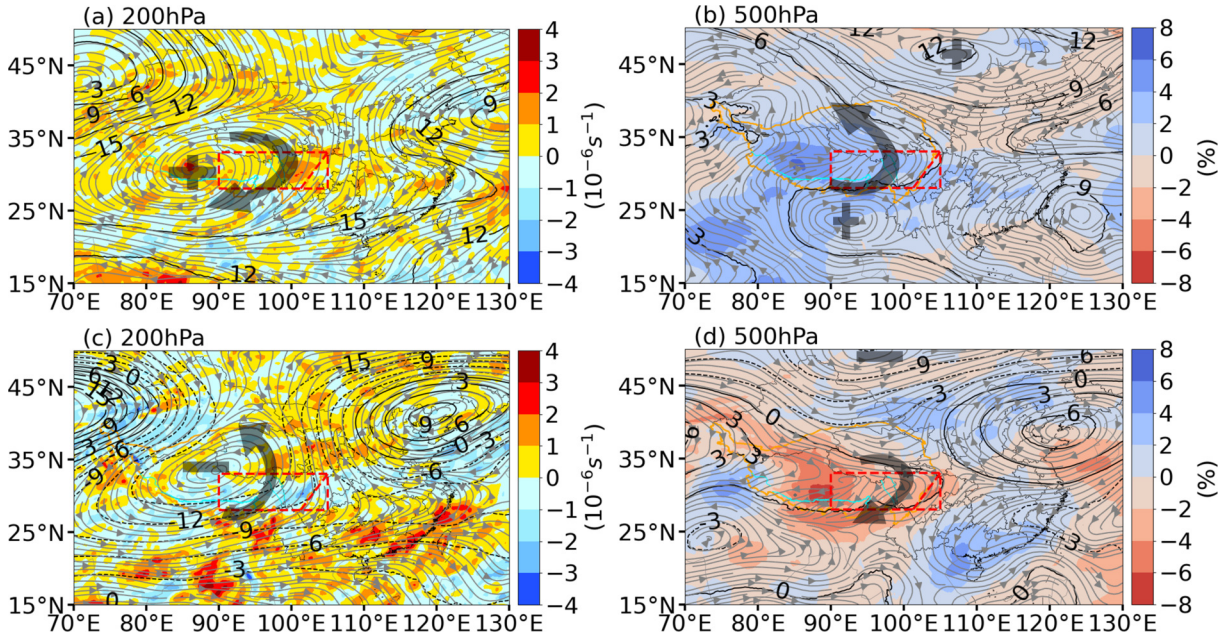

Fig. 4. Composite summer circulation anomalies of heavy and weak SEP years in the CWKR (a–b) correspond to heavy SEP years, and (c–d) correspond to weak SEP years. The pressure level is marked at the upper left of each subplot. The gray streamline is the horizontal circulation anomaly. The black contour is the geopotential height anomaly (units: gpm) with positive (negative) anomalies in solid (dashed) contours. Arrows illustrate the direction of abnormal wind flow, and + and – demonstrate the centers of positive and negative geopotential height anomalies, respectively. The shadings in (a) and (c) are horizontal divergence anomalies and the shadings in (b) and (d) are the relative humidity anomalies indicated by the color bars to the right. Illustration of the KR and other map settings are the same as Fig. 1.

gence over the CWKR (Fig. 4c). At 500 hPa, the cyclonic anomaly in Mongolia helps to establish a geopotential anomaly pattern of "low northeast, high southwest" north of the CWKR, thereby inducing anomalous northwesterly flow and "anticyclonic shear" to suppress the moist southwesterly flow which has the effect of drying the low-level air over the CWKR (Fig. 4d).

In the EKR, the circulation patterns in the heavy SEP years are as follows. At 200 hPa, a strong anticyclonic circulation anomaly dominates the Bohai Sea, which induces easterlies at the middle and lower reaches of Yangtze-River to flow into the EKR, leading to anomalous easterly flow and upper-level positive divergence anomalies in the EKR (Fig. 5a). The 500 hPa pattern is similar to that at 200 hPa in terms of the anticyclonic circulation anomaly and the easterly anomaly of the EKR (Fig. 5b). However, at 850 hPa, under the influence of the upper and middle levels, the anomalous southerly flow in southern China turns cyclonically into anomalous easterly flow and then enters the EKR, thereby leading to wetter low-level air over the EKR (Fig. 5c).

In contrast, during weak SEP years, the circulation patterns are as follows. At 200 hPa, a strong cyclonic circulation anomaly is found over the Hetao area of China, leading to anomalous northwesterly flow in the EKR and a negative divergence anomaly, which is detrimental to upper-level divergence (Fig. 5d). At 500 hPa, the cyclonic circulation anomaly dominates central and eastern China and anomalously northerly flow in the EKR are found (Fig. 5e). At 850 hPa, under the influence of the upper and middle levels, anomalous westerlies in the EKR flow outward and turn anticyclonically towards the south, leading to drier low-level air over the EKR (Fig. 5f). This is in stark contrast with the observed inward flow observed during heavy SEP years in the EKR.

From section 3.2, we found that more than half of all heavy SEP years in the KR occurred in the last decade, during which SEPA peaked in the CWKR, and that the greatest SEPA in the KR occurred in 2020. The reason for this can be revealed through the analysis of the circulation anomalies of the last decade. In doing this, we found a positive divergence anomaly at 200 hPa over the KR (Fig. 6a), anomalous southerly flow and a positive relative humidity anomaly at 500 hPa over the CWKR (Fig. 6b), and a negative relative humidity anomaly at 850 hPa over the EKR (Fig. 6c). Therefore, the strengthening of ascent over the KR and water vapor convergence over the CWKR can explain the fact that the last decade has seen more than half of all heavy SEP years in the KR and a peak in SEPA over the CWKR. In 2020, the ascent and water vapor conditions were more favorable due to the much stronger positive divergence anomaly at 200 hPa (Fig. 6d) and low-level water vapor convergence in both the CWKR and EKR, along with an obvious low-level anomalous basin inflow (Fig. 6f).

From the above analysis, it can be concluded that the circulation anomalies over the Bay of Bengal and Mongolia can influence the SEPA anomaly in the CWKR by affecting the water vapor flux from the Bay of Bengal and low-level shear. Furthermore, the circulation anomalies over the

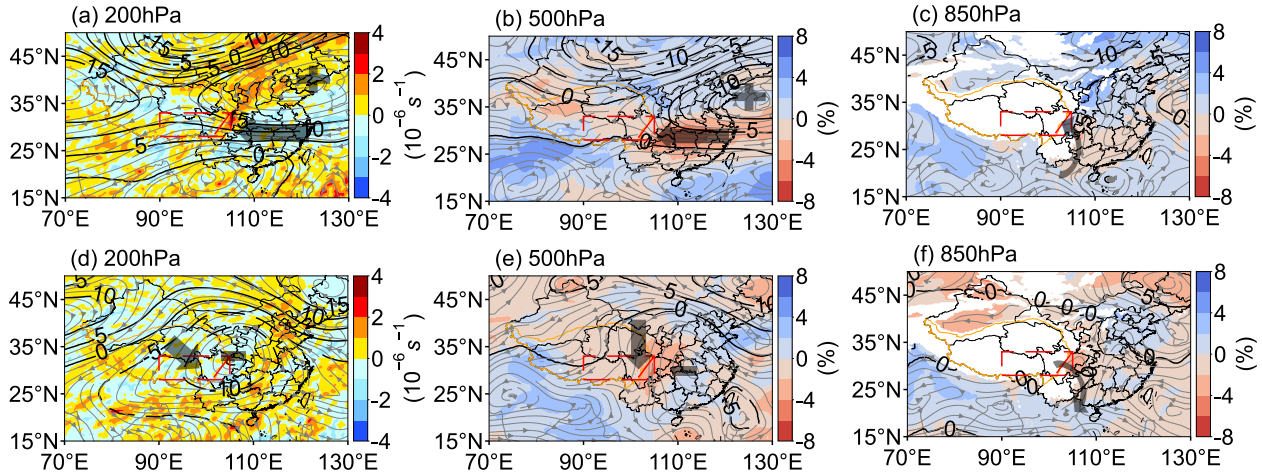

Fig. 5. Composite summer circulation anomalies of heavy and weak SEP years in the EKR. Panels (a–c) correspond to the heavy SEP years, and (d–f) correspond to the weak SEP years. The pressure level is marked at the upper left of each subplot. The plot settings for 200 hPa and 500 hPa are the same as those in Fig. 4, and the plot settings for 850 hPa are the same as 500 hPa except that the white area represents the terrain.

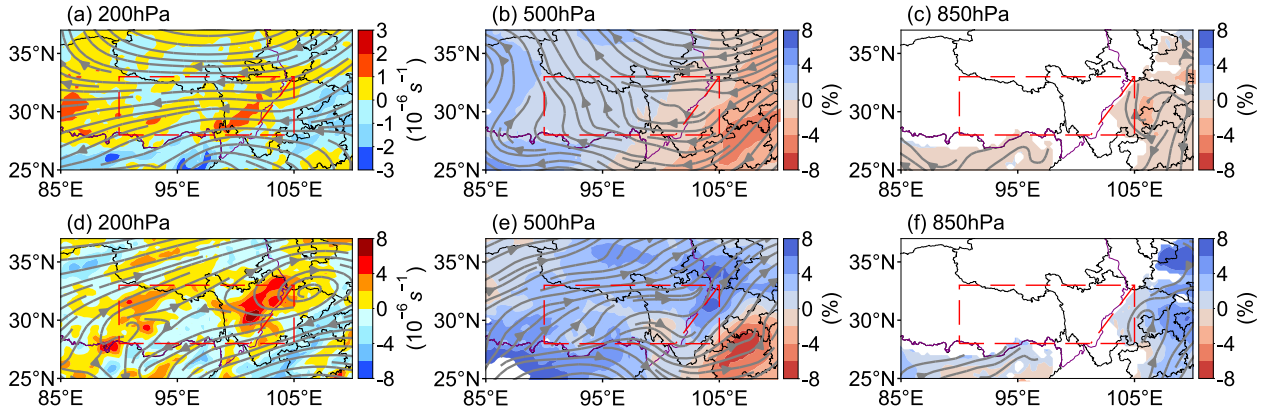

Fig. 6. Composite summer circulation anomalies of 2011–20 and the year 2020 in the KR. Panels (a–c) correspond to 2011–20, and (d–f) correspond to 2020. The pressure levels are marked at the upper left of each subplot. The plot settings for 200 hPa and 500 hPa are the same as those in Fig. 6, and the plot settings for 850 hPa are the same as 500 hPa, except that the white area represents the terrain.

Bohai Sea and Hetao area can influence the SEPA anomaly in the EKR by affecting the water vapor flux towards/into the basin. More than half of all heavy SEP years in the KR and an SEPA peak in the CWKR occurred in the last decade because there is stronger upper-level divergence over the KR and more water vapor over the CWKR compared to climatology. The SEPA peak in 2020 in the KR appears to result from much stronger upper-level divergence over the KR and much more water vapor over the entire KR compared to climatology.

4.2. *The impact of ascent, water vapor convergence, and atmospheric convective instability*

The mechanism for SEPA variation is also greatly affected by ascent (Li and O'Gorman, 2020; Nie et al., 2020), water vapor convergence (Fujita and Sato, 2017; Kunkel et al., 2020), and atmospheric convective instability (Hibino et al., 2018; Nayak and Takemi, 2021).

As shown in Fig. 7, for either the CWKR or EKR, in heavy (weak) SEP years, there is an ascending (descending) vertical motion anomaly below 200 hPa, and the low-level vorticity anomaly is mainly positive (negative), indicating that the ascent is stronger (weaker) than climate mean; the low-level water vapor flux divergence anomaly is negative (positive), indicating that the low-level water vapor convergence is stronger (weaker) than climate mean. The pseudo-equivalent potential temperature (represented by θ_{se}) anomaly of the regional atmosphere is positive (negative), indicating that the atmosphere is warmer and more moist (colder and drier) than the climate mean. Besides, the θ_{se} anomaly has a high absolute value at low levels and a low absolute value at high levels, which is conducive to satisfying $\partial\theta_{se}/\partial z < 0$ ($\partial\theta_{se}/\partial z > 0$), indicating that the atmosphere is more unstable (stable) than the climate mean. These results prove that a strengthened (weakened) ascent, water vapor convergence (divergence), and atmospheric convective instability (stability) are direct factors that cause more (less) SEPA in the KR.

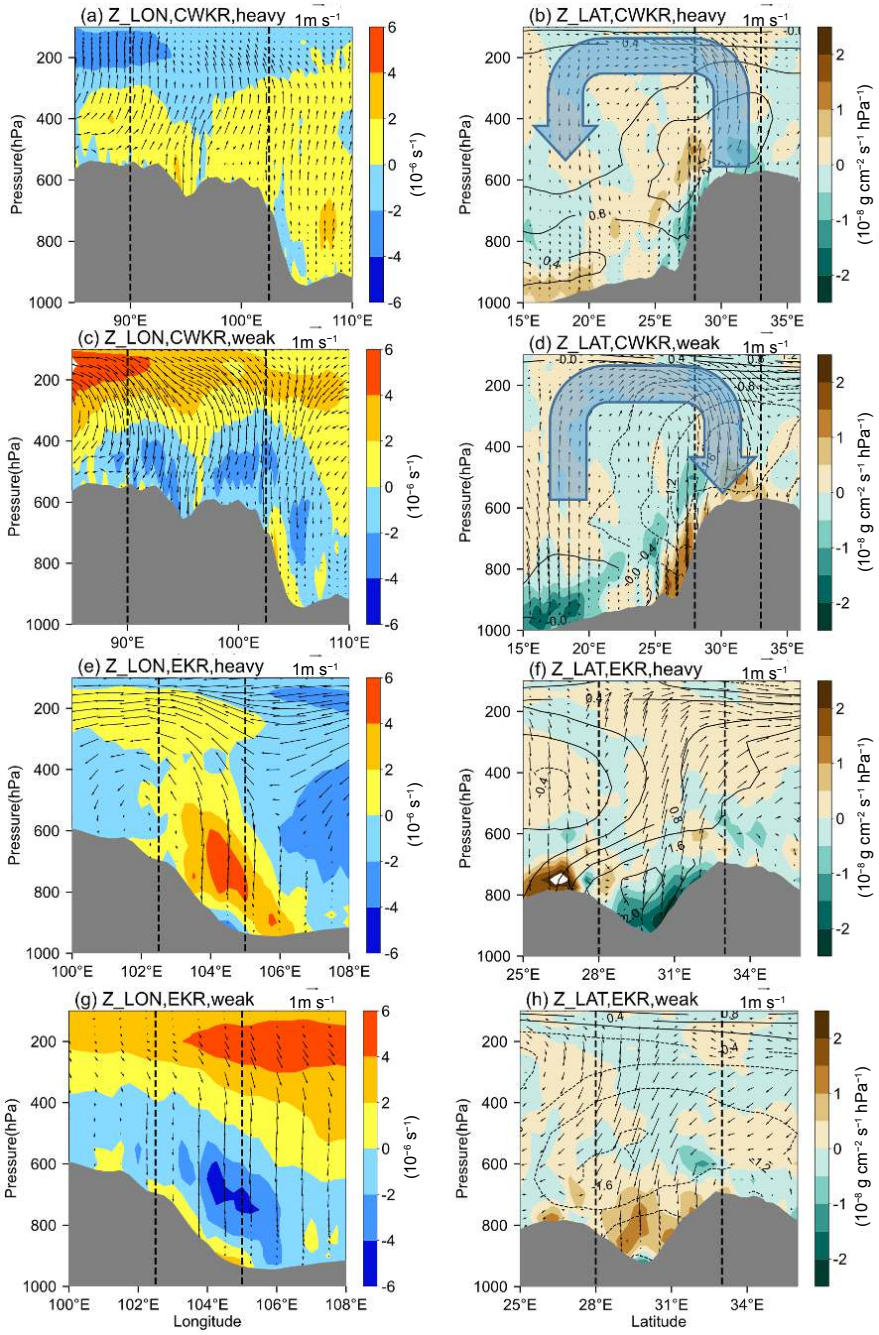

Fig. 7. Vertical cross-sections of composite summer anomalies of the wind field, relative vorticity, water vapor flux divergence and θ_{se} for heavy and weak SEP years in the KR. In each subplot, the title is the cross-section option (Z_LON indicates the height-longitude cross-section, Z_LAT indicates the height-latitude cross-section), (CWKR or EKR) is the study area option, and the composite years are given by heavy, for heavy SEP years, and weak, for weak SEP years. In (a), (c), (e), and (g), the shading represents the relative vorticity anomaly, and the wind field is the composite of the zonal wind u and ω multiplied by –100, all averaged over 28º–33°N. The area 90°–102.5°E within the black dashed lines in (a) and (c) represents the CWKR, while the area 102.5°–105.0°E within the black dashed lines in (e) and (g) represents the EKR. In (b), (d), (f), and (h), the shading represents the water vapor flux divergence anomaly, the wind field is the composite of meridional wind v and ω multiplied by –100, and the contour represents θ_{se} anomaly (units: K), these are all averaged over 90°–102.5°E for (b) and (d) and 102.5°–105°E for (f) and (h), respectively, the area 28°–33°N within the black dashed lines represent the KR. ω is the vertical velocity in pressure coordinates. The thick arrow in (b) and (d) illustrates the abnormal meridional flow. The gray area denotes the terrain.

The ascent anomalies responsible for SEPA variation in the CWKR and EKR are caused by different mechanisms. For the heavy SEP years in the CWKR, the low-level air over the plateau ascends to 200 hPa and turns to the south before it descends over the low-latitude plains (15°–20°N) (Fig. 7b). In weak SEP years, the converse is true; the air ascends over the low-latitude plains and descends over the plateau (Fig. 7d). Previous studies have discovered a closed meridional circulation prevailing to the south of the plateau in summer, with ascending flow over the plateau and descending flow to its south (Yeh et al., 1979; Yang et al., 1992). Therefore, the ascent anomalies in the CWKR are very likely related to the variation of the prevailing meridional circulation south of the plateau in summer. By contrast, in the EKR, it can be seen that the strong positive vorticity anomaly appears narrow and parallel to the terrain, and no vertical circulation is evident (Figs. 7e, g). Previous studies have shown that the higher speed of the upstream wind, the stronger the ascent on the windward slope due to topographic forcing (Snyder et al., 1985; Smith, 1989a, b, 2019). These results indicate that the easterly anomaly helps to strengthen the topographic forcing over the steep slopes, thus strengthening the ascent in the EKR. Therefore, the ascent anomaly for SEPA variation in the CWKR is related to the meridional circulation south of the plateau, while the ascent anomaly for SEPA variation in the EKR is related to the topographic lifting of the easterly anomaly at the steep slope of the eastern plateau.

Based on the results in sections 4.1 and 4.2, it can be concluded that the SEPA variation in the KR is strongly related to the atmospheric circulation, and the impact process differs greatly between the CWKR and EKR. When the 500 hPa pattern over the Bay of Bengal and Mongolia is dominated by anticyclonic circulation anomalies, the low-level southerly and cyclonic shear will be strengthened, favoring more SEPA in the CWKR. When the upper and middle levels over the Bohai Sea are dominated by anticyclonic circulation anomalies, the low-level easterly wind over the basin will be strengthened, favoring more SEPA in the EKR. Strengthened ascents, water vapor convergence, and convective instability are also conducive to more SEPA. While the ascent anomalies in the CWKR may be related to the summer meridional circulation south of the plateau, the ascent anomalies in the EKR may also be related to the topographic forcing of the easterly winds.

5. Summary and discussion

In this study, the spatial-temporal distribution characteristics of SEP in the key region of the Sichuan-Tibet Railway (KR) are revealed using the rain-gauge daily precipitation data from 1979 to 2020. The mechanism of SEPA variation in the KR is investigated by analyzing the circulation, ascent, water vapor convergence, and atmospheric convective instability. The results are as follows:

1) In the past 42 years, SEP in the KR occurred 2.7 d every year and on consecutive days once every 5 years. SEP contributes nearly 30% to summer precipitation in the KR and has a significant nocturnal percentage of nearly 75%. Significant spatial differences of SEP in the KR exist, as R_{95} in the plateau-dominated CWKR and the basin-dominated EKR are without exception, smaller than 25 mm d^{-1} and larger than 25 mm d^{-1}, respectively. Also, SEP in the CWKR is less intense, by nearly 70%, and makes a smaller contribution to summer precipitation, despite having a 20% higher frequency, a slightly higher nocturnal precipitation percentage, and a slightly higher frequency of consecutive occurrence than SEP in the EKR.

2) In the past 42 years, the SEP in the KR increased slightly while SEP in the CWKR increased significantly. More than half of all heavy SEP years in KR occurred during the last decade, and 2020 was the year with the most SEPA in the KR. SEPA in the CWKR also peaked in the last decade.

3) The SEPA variation in the KR is related to atmospheric circulation anomalies. When the 500 hPa pattern over the Bay of Bengal and Mongolia is dominated by anticyclonic circulation anomalies, the low-level southerly and cyclonic shear over the southeastern plateau will be strengthened, favoring more SEPA in the CWKR. When the upper and middle levels over the Bohai Sea are dominated by anticyclonic circulation anomalies, the low-level easterly wind towards the basin will be strengthened, favoring more SEPA in the EKR. The strengthening of the ascent, water vapor convergence, and convective instability is thought to be conducive to more SEPA.

Previous extreme precipitation research mostly focused on either Sichuan province (or the Sichuan Basin) or the Qinghai-Tibet Plateau alone, leaving a lack of clarity for the overall SEP characteristics over the Sichuan-Tibet Railway region as a whole. In this study, we specifically focused on the key region of the Sichuan-Tibet Railway (KR). In doing so, we provided a new picture of various aspects of SEP over the KR, which deepened the scientific understanding of SEP along the railway and will prove helpful in better securing the railway.

We also found that the SEP characteristics exhibit significant differences along the railway and that these differences are closely related to the different physical mechanisms between the plateau and basin areas. Previous studies found that the Qinghai-Tibet Plateau features low water vapor (Zhou and Liu, 1981; Liu et al., 2018) and a high precipitation conversion rate (Cai et al., 2004), the former tending to inhibit precipitation intensity while the latter favoring more rainy days (Fu et al., 2006, 2020), noting that the SEP frequency is proportional (5%) to rainy days. This may explain our finding that SEP over the CWKR is less intense but occurs more frequently than that over the EKR.

Our study stresses the importance of studying the different mechanisms of SEP in the plateau and basin areas, as was noted in previous studies (Deng et al., 2022). For SEP in the basin, the easterly inflow from the south and topo-

graphic effects are very important (Hu et al., 2015; Zhang et al., 2019b). For SEP in the plateau, the shear line is found to be the major influencing synoptic system (Sun et al., 2021), and our study found that anomalous low-level cyclonic shear, which may present itself as the strengthening of the shear line due to low-level turbulence, plays an important role.

It is noteworthy that the Nyingchi-Lhasa and Ya'an-Nyingchi sections of the Sichuan-Tibet Railway are both located in the CWKR, where the increase in SEPA in the last decade is most obvious, suggesting a potential increase in SEPA in the CWKR in the future. Therefore, SEP in the CWKR should attract more research attention. In addition, the impact mechanism of the topography and the effects of meridional circulation upon the ascent needs to be further investigated.

Acknowledgements. This study was supported by the Key Program of the National Science Foundation of China (Grant No. 42030611), the Second Tibetan Plateau Scientific Expedition and Research (STEP) program (Grant No. 2019QZKK0105), and the Integration Project of the Major Research Program of the National Natural Science Foundation of China (Grant No. 91937301).

APPENDIX

Abbreviations and Symbols

KR	Key region
CWKR	Central-western KR
EKR	Eastern KR
EBP	The eastern boundary of the plateau
SEP	Summertime extreme precipitation
SEPA	Summertime extreme precipitation amount
SEPD	Summertime extreme precipitation day
SEPI	Summertime extreme precipitation intensity
AC	Anticyclonic circulation
WPSH	West Pacific Subtropical High
R_n	Percentage of nighttime precipitation in SEP
R_{SEP}	Percentage of SEPA in summertime total precipitation amount
N_{CE}	The number of consecutive SEP events
θ_{se}	Pseudo-equivalent potential temperature

REFERENCES

Cai, Y., Z. A. Qian, T. W. Wu, X. Y. Liang, and M. H. Song, 2004: Distribution, changes of atmospheric precipitable water over Qinghai-Xizang Plateau and its surroundings and their changeable precipitation climate. *Plateau Meteorology*, **23**(1), 1–10, https://doi.org/10.3321/j.issn:1000-0534.2004.01.001. (in Chinese with English abstract)

Chen, Q. L., X. R. Liu, G. Z. Fan, and W. Hua, 2010: Features of summer precipitation change over the West Sichuan Plateau and its relationship with large-scale circulations. *Journal of Desert Research*, **30**(3), 706–711. (in Chinese with English abstract)

Deng, M. Y., R. Y. Lu, and C. F. Li, 2022: Contrasts between the interannual variations of extreme rainfall over western and eastern Sichuan in mid-summer. *Adv. Atmos. Sci.*, **39**(6), 999–1011, https://doi.org/10.1007/s00376-021-1219-3.

Ding, J., L. Cuo, Y. X. Zhang, C. J. Zhang, L. Q. Liang, and Z. Liu, 2021: Annual and seasonal precipitation and their extremes over the Tibetan Plateau and its surroundings in 1963–2015. *Atmosphere*, **12**(5), 620, https://doi.org/10.3390/atmos12050620.

Du, H. B., and Coauthors, 2022: Extreme precipitation on consecutive days occurs more often in a warming climate. *Bull. Amer. Meteor. Soc.*, **103**(4), E1130–E1145, https://doi.org/10.1175/BAMS-D-21-0140.1.

Feng, L., and F. Y. Wei, 2008: Regional characteristics of summer precipitation on Tibetan Plateau and it's water vapor feature in neighboring areas. *Plateau Meteorology*, **27**(3), 491–499. (in Chinese with English abstract)

Fu, Y., G. S. Liu, G. X. Wu, R. C. Yu, Y. P. Xu, Y. Wang, R. Li, and Q. Liu, 2006: Tower mast of precipitation over central Tibetan plateau summer. *Geophysical Research Letters*, **33**, L05802, https://doi.org/10.1029/2005GL024713.

Fu, Y., Y. M. Ma, L. Zhong, Y. J. Yang, X. L. Guo, C. H. Wang, X. F. Xu, K. Yang, X. D. Xu, L. P. Liu, G. Z. Fan, Y. Q. Li, and D. H. Wang, 2020: Land-surface processes and summer-cloud-precipitation characteristics in the Tibetan Plateau and their effects on downstream weather: a review and perspective. *Natl Sci Rev*, **7**, 500–515, https://doi.org/10.1093/nsr/nwz226.

Fujita, M., and T. Sato, 2017: Observed behaviours of precipitable water vapour and precipitation intensity in response to upper air profiles estimated from surface air temperature. *Scientific Reports*, **7**, 4233, https://doi.org/10.1038/s41598-017-04443-9.

Gao, Y. H., L. Cuo, and Y. X. Zhang, 2014: Changes in moisture flux over the Tibetan Plateau during 1979-2011 and possible mechanisms. *J. Climate*, **27**(5), 1876–1893, https://doi.org/10.1175/JCLI-D-13-00321.1.

He, B. R., and P. M. Zhai, 2018: Changes in persistent and non-persistent extreme precipitation in China from 1961 to 2016. *Advances in Climate Change Research*, **9**(3), 177–184, https://doi.org/10.1016/j.accre.2018.08.002.

Hegerl, G. C., and Coauthors, 2019: Causes of climate change over the historical record. *Environmental Research Letters*, **14**(12), 123006, https://doi.org/10.1088/1748-9326/ab4557.

Hibino, K., I. Takayabu, Y. Wakazuki, and T. Ogata, 2018: Physical responses of convective heavy rainfall to future warming condition: Case study of the Hiroshima Event. *Frontiers in Earth Science*, **6**, 35, https://doi.org/10.3389/feart.2018.00035.

Hu, D., and Y. Q. Li, 2015: Spatial and temporal variations of nocturnal precipitation in Sichuan over the eastern Tibetan Plateau. *Chinese Journal of Atmospheric Sciences*, **39**(1), 161–179, https://doi.org/10.3878/j.issn.1006-9895.1405.13307. (in Chinese with English abstract)

Hu, Y. M., P. M. Zhai, L. H. Liu, Y. Chen, and Y. J. Liu, 2015: Dominant large-scale atmospheric circulation systems for the extreme precipitation over the western Sichuan Basin in summer 2013. *Advances in Meteorology*, **2015**, 690363, https://doi.org/10.1155/2015/690363.

Huang, J., S. L. Sun, Y. Xue, J. J. Li, and J. C. Zhang, 2014: Spatial and temporal variability of precipitation and dryness/wetness during 1961–2008 in Sichuan Province, West China. *Water Resources Management*, **28**, 1655–1670, https://doi.org/10.

1007/s11269-014-0572-8.

Kundzewicz, Z. W., and Coauthors, 2005: Summer floods in Central Europe – Climate change track? *Natural Hazards*, **36**(1), 165–189, https://doi.org/10.1007/s11069-004-4547-6.

Kunkel, K. E., S. E. Stevens, L. E. Stevens, and T. R. Karl, 2020: Observed climatological relationships of extreme daily precipitation events with precipitable water and vertical velocity in the contiguous United States. *Geophys. Res. Lett.*, **47**(12), e2019GL086721, https://doi.org/10.1029/2019GL086721.

Li, J., W. J. Dong, and Z. W. Yan, 2012: Changes of climate extremes of temperature and precipitation in summer in eastern China associated with changes in atmospheric circulation in East Asia during 1960–2008. *Chinese Science Bulletin*, **57**(15), 1856–1861, https://doi.org/10.1007/s11434-012-4989-2.

Li, J., Y. D. Zhao, and J. Iqbal, 2019: Variation patterns of extreme precipitation and relation to ocean-atmospheric climate in Sichuan province China from 1961 to 2017. *Theor. Appl. Climatol.*, **137**, 3009–3026, https://doi.org/10.1007/s00704-019-02792-1.

Li, L., S. Yang, Z. Y. Wang, X. D. Zhu, and H. Y. Tang, 2010: Evidence of warming and wetting climate over the Qinghai-Tibet Plateau. *Arctic, Antarctic, and Alpine Research*, **42**(4), 449–457, https://doi.org/10.1657/1938-4246-42.4.449.

Li, Z. W., and P. A. O'Gorman, 2020: Response of vertical velocities in extratropical precipitation extremes to climate change. *J. Climate*, **33**, 7125–7139, https://doi.org/10.1175/JCLI-D-19-0766.1.

Liu, K., M. Wang, and T. J. Zhou, 2021: Increasing costs to Chinese railway infrastructure by extreme precipitation in a warmer world. *Transportation Research Part D: Transport and Environment*, **93**, 102797, https://doi.org/10.1016/j.trd.2021.102797.

Liu, W. B., L. Wang, D. L. Chen, K. Tu, C. Q. Ruan, and Z. Y. Hu, 2016: Large-scale circulation classification and its links to observed precipitation in the eastern and central Tibetan Plateau. *Climate Dyn.*, **46**, 3481–3497, https://doi.org/10.1007/s00382-015-2782-z.

Liu, Y. M., Y. F. Yan, J. H. Lü, and X. L. Liu, 2018: Review of current investigations of cloud, radiation and rainfall over the Tibetan Plateau with the CloudSat/CALIPSO dataset. *Chinese Journal of Atmospheric Sciences*, **42**(4), 847–858, https://doi.org/10.3878/j.issn.1006-9895.1805.17281. (in Chinese with English abstract)

Lu, C. F., and C. X. Cai, 2019: Challenges and countermeasures for construction safety during the Sichuan–Tibet Railway Project. *Engineering*, **5**(5), 833–838, https://doi.org/10.1016/j.eng.2019.06.007.

Lu, S., Z. Y. Hu, H. P. Yu, W. W. Fan, C. W. Fu, and D. Wu, 2021: Changes of extreme precipitation and its associated mechanisms in Northwest China. *Adv. Atmos. Sci.*, **38**(10), 1665–1681, https://doi.org/10.1007/s00376-021-0409-3.

Myhre, G., and Coauthors, 2019: Frequency of extreme precipitation increases extensively with event rareness under global warming. *Scientific Reports*, **9**(1), 16063, https://doi.org/10.1038/s41598-019-52277-4.

Nayak, S., and T. Takemi, 2021: Atmospheric driving mechanisms of extreme precipitation events in July of 2017 and 2018 in western Japan. *Dyn. Atmos. Oceans*, **93**, 101186, https://doi.org/10.1016/j.dynatmoce.2020.101186.

Nie, J., P. X. Dai, and A. H. Sobel, 2020: Dry and moist dynamics shape regional patterns of extreme precipitation sensitivity. *Proceedings of the National Academy of Sciences of the United States of America*, **117**, 8757–8763, https://doi.org/10.1073/pnas.1913584117.

O'Gorman, P. A., and T. Schneider, 2009: The physical basis for increases in precipitation extremes in simulations of 21st-century climate change. *Proceedings of the National Academy of Sciences of the United States of America*, **106**(35), 14 773–14 777, https://doi.org/10.1073/pnas.0907610106.

Palin, E. J., I. S. Oslakovic, K. Gavin, and A. Quinn, 2021: Implications of climate change for railway infrastructure. *WIREs Climate Change*, **12**(5), e728, https://doi.org/10.1002/wcc.728.

Pan, X., Y. F. Fu, S. Yang, Y. Gong, and D. Q. Li, 2021: Diurnal variations of precipitation over the steep slopes of the Himalayas observed by TRMM PR and VIRS. *Adv. Atmos. Sci.*, **38**(4), 641–660, https://doi.org/10.1007/s00376-020-0246-9.

Shi, P. J., and W. T. Yang, 2020: Compound effects of earthquakes and extreme weathers on geo-hazards in mountains. *Climate Change Research*, **16**(4), 405–414, https://doi.org/10.12006/j.issn.1673-1719.2019.174. (in Chinese with English abstract)

Smith, R. B., 1989a: Hydrostatic airflow over mountains. *Advances in Geophysics*, **31**, 1–41, https://doi.org/10.1016/S0065-2687(08)60052-7.

Smith, R. B., 1989b: Mountain-induced stagnation points in hydrostatic flow. *Tellus A*, **41**, 270–274, https://doi.org/10.3402/tellusa.v41i3.11839.

Smith, R. B., 2019: 100 years of progress on mountain meteorology research. *Meteor. Monogr.*, **59**, 20.1–20.73, https://doi.org/10.1175/AMSMONOGRAPHS-D-18-0022.1.

Snyder, W. H., R. S. Thompson, R. E. Eskridge, R. E. Lawson, I. P. Castro, J. T. Lee, J. C. R. Hunt, and Y. Ogawa, 1985: The structure of strongly stratified flow over hills: Dividing-streamline concept. *J. Fluid Mech.*, **152**, 249–288, https://doi.org/10.1017/S0022112085000684.

Sun, J., and F. Q. Zhang, 2017: Daily extreme precipitation and trends over China. *Science China Earth Sciences*, **60**(12), 2190–2203, https://doi.org/10.1007/s11430-016-9117-8.

Sun, J., X. P. Yao, G. W. Deng, and Y. Liu, 2021: Characteristics and synoptic patterns of regional extreme rainfall over the Central and Eastern Tibetan Plateau in boreal summer. *Atmosphere*, **12**(3), 379, https://doi.org/10.3390/atmos12030379.

Sun, J., K. Yang, W. D. Guo, Y. Wang, J. He, and H. Lu, 2020: Why has the Inner Tibetan Plateau become wetter since the Mid-1990s? *J. Climate*, **33**(19), 8507–8522, https://doi.org/10.1175/JCLI-D-19-0471.1.

Tang, G. A., 2019: China Digital Elevation Map (1KM). National Data Center for Qinghai-Tibet Plateau Science. [Available online from http://www.tpdc.ac.cn/zh-hans/data/12e91073-0181-44bf-8308-c50e5bd9a734/]

Webster, P. J., V. E. Toma, and H.-M. Kim, 2011: Were the 2010 Pakistan floods predictable. *Geophys. Res. Lett.*, **38**(4), L04806, https://doi.org/10.1029/2010GL046346.

Xiong, J. N., Z. W. Yong, Z. G. Wang, W. M. Cheng, Y. Li, H. Zhang, C. C. Ye, and Y. M. Yang, 2019: Spatial and temporal patterns of the extreme precipitation across the Tibetan Plateau (1986–2015). *Water*, **11**(7), 1453, https://doi.org/10.3390/w11071453.

Xue, Y. G., F. M. Kong, S. C. Li, Q. S. Zhang, D. H. Qiu, M. X. Su, and Z. Q. Li, 2021: China starts the world's hardest "Sky-High Road" project: Challenges and countermeasures for

Sichuan-Tibet railway. *Innovation*, **2**(2), 100105, https://doi.org/10.1016/j.xinn.2021.100105.

Yang, W. Y., D. Z. Ye, and G. X. Wu, 1992: The influence of the Tibetan Plateau on the thermal and circulation fields over East Asia in summer II: Main features of the local circulation fields and the large-scale vertical circulation fields. *Scientia Atmospherica Sinica*, **16**, 287–301, https://doi.org/10.3878/j.issn.1006-9895.1992.03.05. (in Chinese with English abstract)

Yao, S. B., D. B. Jiang, and G. Z. Fan, 2017: Seasonality of precipitation over China. *Chinese Journal of Atmospheric Sciences*, **41**(6), 1191–1203, https://doi.org/10.3878/j.issn.1006-9895.1703.16233. (in Chinese with English abstract)

Yeh, T. C, G. J. Yang, and X. D. Wang, 1979: The average vertical circulations over the East-Asia and the Pacific area, (I) In Summer. *Scientia Atmospherica Sinica*, **3**, 1–11. (in Chinese with English abstract)

You, Q. L., S. C. Kang, E. Aguilar, and Y. P. Yan, 2008: Changes in daily climate extremes in the eastern and central Tibetan Plateau during 1961–2005. *J. Geophys. Res.*, **113**(D7), D07101, https://doi.org/10.1029/2007JD009389.

Zhai, P. M., and X. H. Pan, 2003: Change in extreme temperature and precipitation over northern China during the second half of the 20th Century. *Acta Geographica Sinica*, **58**(Z1), 1–10, https://doi.org/10.3321/j.issn:0375-5444.2003.z1.001. (in Chinese with English abstract)

Zhai, P. M., X. B. Zhang, H. Wan, and X. H. Pan, 2005: Trends in total precipitation and frequency of daily precipitation extremes over China. *J. Climate*, **18**(7), 1096–1108, https://doi.org/10.1175/JCLI-3318.1.

Zhang, J. P., T. B. Zhao, L. B. Zhou, and L. K. Ran, 2021: Historical changes and future projections of extreme temperature and precipitation along the Sichuan–Tibet Railway. *J. Meteor. Res.*, **35**(3), 402–415, https://doi.org/10.1007/s13351-021-0175-2.

Zhang, X., X. P. Yao, J. L. Ma, and Z. G. Mima, 2016: Climatology of transverse shear lines related to heavy rainfall over the Tibetan Plateau during boreal summer. *J. Meteor. Res.*, **30**(6), 915–926, https://doi.org/10.1007/s13351-016-6952-7.

Zhang, X. B., L. Alexander, G. C. Hegerl, P. Jones, A. K. Tank, T. C. Peterson, B. Trewin, and F. W. Zwiers, 2011: Indices for monitoring changes in extremes based on daily temperature and precipitation data. *WIREs Climate Change*, **2**(6), 851–870, https://doi.org/10.1002/wcc.147.

Zhang, Y., H. X. Ren, and X. D. Pan, 2019a: Integration dataset of Tibet Plateau boundary. National Tibetan Plateau Data Center, doi: 10.11888/Geogra.tpdc.270099.CSTR:18406.11.Geogra.tpdc.270099. [Available online from http://data.tpdc.ac.cn/zh-hans/data/61701a2b-31e5-41bf-b0a3-607c2a9bd3b3/]

Zhang, Y. H., M. Xue, K. F. Zhu, and B. W. Zhou, 2019b: What is the main cause of diurnal variation and nocturnal peak of summer precipitation in Sichuan Basin, China? The key role of boundary layer low-level jet inertial oscillations *J. Geophys. Res.: Atmos.*, **124**(5), 2643–2664, https://doi.org/10.1029/2018JD029834.

Zhao, D., L. X. Zhang, and T. J. Zhou, 2022: Detectable anthropogenic forcing on the long-term changes of summer precipitation over the Tibetan Plateau. *Climate Dyn.*, **59**, 1939–1952, https://doi.org/10.1007/s00382-022-06189-1.

Zhao, W. H., and Coauthors, 2018: Declining hailstorm frequency in China during 1961–2015 and its potential influential factors. *International Journal of Climatology*, **38**(11), 4116–4126, https://doi.org/10.1002/joc.5556.

Zhou, J. S., and H. L. Liu, 1981: The basic features of distribution of water vapour content and their controlling factors in China. *Acta Geographica Sinica*, **36**(4), 377–391, https://doi.org/10.11821/xb198104004. (in Chinese)

Zhou, T. J., and Coauthors, 2022: 2021: A year of unprecedented climate extremes in Eastern Asia, North America, and Europe. *Adv. Atmos. Sci.*, **39**, 1598–1607, https://doi.org/10.1007/S00376-022-2063-9.

Zhu, L. P., and Coauthors, 2015: Climate change on the Tibetan Plateau in response to shifting atmospheric circulation since the LGM. *Scientific Reports*, **5**, 13318, https://doi.org/10.1038/srep13318.